$Rb_3B_5O_8F_2$ and $K_{0.6}Rb_{2.4}B_5O_8F_2$: two new deep-ultraviolet transparent nonlinear optical fluorooxoborates designed by cations regulation

Ruonan Zhang,‡[a,b] Bingliang Cheng,‡[a,b] Xuping Wang,[a] Rong Yang,[a,b] Zhihua Yang,[a] Shujuan Han*[a] and Shilie Pan*[a]
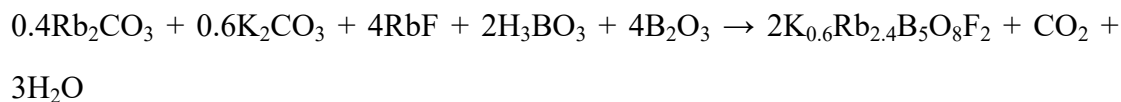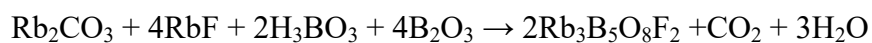
[a]Research Center for Crystal Materials; CAS Key Laboratory of Functional Materials and Devices for Special Environments; Xinjiang Technical Institute of Physics and Chemistry, CAS, 40-1 South Beijing Road, Urumqi 830011, China. E-mails: hansj@ms.xjb.ac.cn, slpan@ms.xjb.ac.cn.

[b]Center of Materials Science and Optoelectronics Engineering, University of Chinese Academy of Sciences, Beijing 100049, China

Experimental Section

Synthesis. Crystals of $Rb_3B_5O_8F_2$ and $K_{0.6}Rb_{2.4}B_5O_8F_2$ were grown by the high-temperature solution method in a closed system. A mixture of RbF, B_2O_3 and $RbNO_3$ at a ratio of 1: 1.1: 0.5 for $Rb_3B_5O_8F_2$ and a mixture of $RbBF_4$, Rb_2CO_3, KF and B_2O_3 with a ratio of 1: 2: 2: 4 for $K_{0.6}Rb_{2.4}B_5O_8F_2$ were mixed in an agate mortar, and then moved to a tidy quartz tube (Φ10 mm × 100 mm), respectively. The tubes were flame-sealed under 10^{-3} Pa. The samples were gradually heated to a specified temperature (350 ºC for $Rb_3B_5O_8F_2$ and 430 ºC for $K_{0.6}Rb_{2.4}B_5O_8F_2$) in 10 h and held at the temperature for 48 h, then cooled 100 ºC in 100 h, and then cooled to room temperature at a rate of 15 °C/h. Small crystals of the above compounds were found in the tubes after growth and several single crystals were picked up for further single-crystal X-ray diffraction measurements, respectively.

Polycrystalline samples of $Rb_3B_5O_8F_2$ and $K_{0.6}Rb_{2.4}B_5O_8F_2$ were synthesized by conventional solid-state reactions in the open air based on the following reaction:

$Rb_2CO_3 + 4RbF + 2H_3BO_3 + 4B_2O_3 \rightarrow 2Rb_3B_5O_8F_2 + CO_2 + 3H_2O$

$0.4Rb_2CO_3 + 0.6K_2CO_3 + 4RbF + 2H_3BO_3 + 4B_2O_3 \rightarrow 2K_{0.6}Rb_{2.4}B_5O_8F_2 + CO_2 + 3H_2O$

Stoichiometric amounts of raw materials above were ground thoroughly and placed into alumina crucibles, respectively. The alumina crucibles were heated to 300 ºC for 10 h to decompose CO_2 and H_2O, and then the temperature was raised to 400 ºC and held for 5 days with several intermittent grindings. The phase purity of $Rb_3B_5O_8F_2$ and $K_{0.6}Rb_{2.4}B_5O_8F_2$ was confirmed by powder X-ray diffraction (XRD) pattern.

Single-Crystal X-ray Diffraction. The single-crystal XRD data were collected on a Bruker D8 Venture diffractometer assembled with monochromatic Mo-Kα (λ = 0.71073 Å) as the radiation source at room temperature and then integrated by using the SAINT program.[1] All the structures were solved by direct methods and refined through the full-matrix least-squares fitting on F_2 with the OLEX2 software.[2] These structures were verified utilizing the ADDSYM algorithm from PLATON.[3] The final refined atomic positions and isotropic thermal parameters, selected bond lengths, and

angles for the title compounds are given in Tables S2–S5. The structural rationality of the title compounds is also evident from bond valence sum (BVS) calculations (Table S2‒S3).

Powder X-ray Diffraction. Powder XRD data were collected with a Bruker D2 PHASER diffractometer equipped with Cu Kα radiation (λ = 1.5418 Å) at room temperature. Data were collected in the angular (2θ) ranging from 10 to 70 ° with a scan step width and a fixed counting time of 0.02 ° and 1 s/step, respectively.

Energy Dispersive X-ray (EDX) Spectroscope. EDX spectroscope was measured on a SUPRA 55VP field emission scanning electron microscope equipped with a BRUKER X-ray Flash-SDD-5010 energy-dispersive X-ray spectroscope.

Thermal Analysis. Thermogravimetric analyses (TGA) and differential scanning calorimetry (DSC) were measured on a NETZSCH STA 449 F3 simultaneous analyzer instrument. The polycrystalline powders were placed in a Pt crucible and heated from room temperature to 800 °C at a rate of 5 °C·min^{-1} under a constant flow of nitrogen gas.

Infrared Spectroscopy. The infrared spectra were recorded using a Shimadzu IRAffinity-1 Fourier transform infrared spectrometer within the range of 400–4000 cm^{-1}. The sample was mixed with dried KBr.

UV−Vis−NIR Diffuse Reflectance Spectroscopy. The diffuse reflectance spectra were measured by using a Shimadzu Solid Spec-3700 DUV spectrophotometer in the wavelength range of 200–2600 nm at room temperature.

Second-Order NLO Measurements. Powder SHG measurements of the two compounds were operated by the Kurtz−Perry method[4] using a Q-switched Nd: YVO$_4$ solid-state laser at 1064 nm. The polycrystalline powders were ground and divided into the different particle size ranges: 38−55, 55−88, 88−105, 105−155, 155-200 and 200−250 μm. The samples were pressed between glass slides, and secured in 1 mm thick aluminum holders with an 8 mm diameter hole. Microcrystallines of KDP were also sieved into the same particle size range and used as references.

Computational Methods. The electronic and band structures of title compounds were calculated using a plane-wave pseudo-potential total energy package, CASTEP.[5]

The theoretical basis of CASTEP is density functional theory,[6] and the generalized gradient approximation (GGA) with the Perdew-Burke-Emzerhof (PBE) exchange-correlation functional[7] was chosen for all calculations. Adopting the norm-conserving pseudopotential (NCP),[8,9] the following orbital electrons were treated as valence electrons: Rb: $4s^2\ 4p^6\ 5s^1$, B: $2s^2\ 2p^1$, O: $2s^2\ 2p^4$ and F: $2s^2\ 2p^5$. Besides, the kinetic energy cutoffs were chosen as 940.0 eV, and the k-point separation was set as 0.05 Å^{-1} in the Brillouin zone. The other calculation parameters and convergence criteria were the default values of the CASTEP code. It is well-known that GGA usually underestimates the band gap owing to the discontinuity of the exchange-correlation energy functional. Therefore, the HSE06 was adopted to afford more precise band gap values.

Results and Discussion

Table S1. Crystal data and structure refinement for $Rb_3B_5O_8F_2$ and $K_{0.6}Rb_{2.4}B_5O_8F_2$.

Empirical formula	$Rb_3B_5O_8F_2$	$K_{0.6}Rb_{2.4}B_5O_8F_2$
Formula weight	476.46	448.64
Temperature	273.15 K	273.15 K
Wavelength	0.71073 Å	0.71073 Å
Crystal system, space group	Monoclinic, $P2_1$	Monoclinic, $P2_1$
Unit cell dimensions	$a = 6.7342(4)$ Å	$a = 6.7132(6)$ Å
	$b = 7.0706(4)$ Å $\beta = 93.593(2)°$	$b = 6.9794(7)$ Å $\beta = 94.099(4)°$
	$c = 10.0108(6)$ Å	$c = 9.9534(11)$ Å
Volume	475.73(5) Å^3	465.16(8) Å^3
Z, Calculated density	2, 3.326 g/cm^3	2, 3.203 g/cm^3
Absorption coefficient	15.427 mm^{-1}	12.927 mm^{-1}
$F(000)$	436	414
θ range for data collection	2.038 to 27.496°	2.051 to 27.562°
Limiting indices	$-8 \leq h \leq 8$, $-9 \leq k \leq 9$, $-12 \leq l \leq 12$	$-7 \leq h \leq 8$, $-9 \leq k \leq 9$, $-12 \leq l \leq 12$
Reflections collected / unique	8119 / 2158 [R(int) = 0.0431]	5857 / 2127 [R(int) = 0.0691]
Completeness	99.5	99.8
Maximum and minimum transmission	0.7456 and 0.5339	0.7456 and 0.5865
Refinement method	Full matrix least squares on F^2	Full matrix least squares on F^2
Data / restraints / parameters	2158 / 1 / 164	2127 / 1 / 163
Goodness-of-fit on F^2	0.950	0.954
Final R indices [$F_o^2 > 2\sigma(F_o^2)$][a]	$R_1 = 0.0227$, $wR_2 = 0.0427$	$R_1 = 0.0396$, $wR_2 = 0.0706$

R indices (all data)[a]	$R_1 = 0.0256$, $wR_2 = 0.0435$	$R_1 = 0.0466$, $wR_2 = 0.0744$
Absolute structure parameter	0.021(12)	0.023(15)
Largest diff. peak and hole	0.603 and -0.528 e $Å^{-3}$	0.613 and -0.628 e $Å^{-3}$

[a]$R_1 = \Sigma||F_o| - |F_c||/\Sigma|F_o|$ and $wR_2 = [\Sigma w(F_o^2 - F_c^2)^2/\Sigma wF_o^4]^{1/2}$ for $F_o^2 > 2\sigma(F_o^2)$

Table S2. Atomic coordinates ($\times$ 10^4) and equivalent isotropic displacement parameters ($\text{Å}^2 \times 10^3$) for $Rb_3B_5O_8F_2$. U_{eq} is defined as one-third of the trace of the orthogonalized U_{ij} tensor.

atom	x	y	z	U_{eq} (Å^2)	occupancy	BVS
Rb(1)	2960(1)	2082(1)	5020(1)	22(1)	1	0.95
Rb(2)	4089(1)	860(1)	8474(1)	18(1)	1	1.36
Rb(3)	9211(1)	9141(1)	9050(1)	21(1)	1	1.05
B(1)	2083(10)	6855(8)	6114(7)	13(1)	1	3.10
B(2)	2137(10)	7334(8)	3562(7)	14(1)	1	2.99
B(3)	474(10)	4415(8)	7443(6)	11(1)	1	3.00
B(4)	3511(10)	6065(9)	8377(6)	13(1)	1	2.97
B(5)	6978(10)	4839(8)	8020(6)	13(1)	1	3.09
O(1)	3245(7)	7357(5)	7243(4)	20(1)	1	2.05
O(2)	653(6)	5533(5)	6196(4)	18(1)	1	2.12
O(3)	2446(7)	7798(5)	4978(4)	16(1)	1	1.93
O(4)	150(6)	7487(5)	2945(4)	12(1)	1	1.91
O(5)	2352(6)	4380(5)	8230(4)	12(1)	1	2.14
O(6)	5618(6)	5788(6)	8729(4)	16(1)	1	2.08
O(7)	6404(6)	3479(5)	7108(4)	16(1)	1	2.08
O(8)	8927(6)	5314(5)	8241(4)	15(1)	1	2.08
F(1)	2768(5)	5364(4)	3400(4)	21(1)	1	1.09
F(2)	2834(5)	7142(5)	9553(3)	18(1)	1	1.08

Table S3. Atomic coordinates ($\times 10^4$) and equivalent isotropic displacement parameters ($\text{Å}^2 \times 10^3$) for $K_{0.6}Rb_{2.4}B_5O_8F_2$. U_{eq} is defined as one-third of the trace of the orthogonalized U_{ij} tensor.

atom	x	y	z	U_{eq} (Å^2)	occupancy	BVS
Rb(1)	7043(2)	2028(1)	4953(1)	21(1)	1	0.98
Rb(2)	745(2)	9150(2)	958(1)	22(1)	1	1.16
K(3)/Rb(3)	5881(2)	851(2)	1518(2)	21(1)	0.6/0.4	1.27
B(1)	3037(15)	4798(15)	1971(11)	12(2)	1	3.07
B(2)	6518(16)	6040(15)	1594(10)	12(2)	1	3.00
B(3)	9524(14)	4371(15)	2562(10)	9(2)	1	3.03
B(4)	7914(14)	6855(16)	3881(11)	12(2)	1	3.11
B(5)	7847(16)	7267(16)	6448(11)	14(2)	1	2.98
O(1)	1063(9)	5324(9)	1771(7)	15(2)	1	2.07
O(2)	3603(9)	3439(10)	2863(7)	16(2)	1	2.17
O(3)	4366(9)	5783(10)	1237(6)	15(1)	1	1.99
O(4)	7634(9)	4336(9)	1753(6)	13(1)	1	2.06
O(5)	6782(10)	7383(9)	2726(7)	17(2)	1	1.93
O(6)	9317(10)	5479(9)	3808(6)	17(2)	1	2.10
O(7)	7498(10)	7754(9)	5019(6)	13(1)	1	2.10
O(8)	9837(9)	7419(9)	7073(7)	12(2)	1	1.90
F(1)	7151(7)	7119(8)	399(5)	17(1)	1	1.04
F(2)	7194(8)	5293(8)	6614(6)	19(1)	1	1.05

Table S4. Selected bond lengths (Å) and angles (deg.) for $Rb_3B_5O_8F_2$.

Rb(1)-F(1)	2.829(3)	Rb(3)-O(6)	3.388(4)
Rb(1)-O(3)#2	3.049(4)	Rb(3)-O(4)#5	3.143(4)
Rb(1)-O(3)#1	3.135(5)	Rb(3)-O(5)#7	2.985(4)
Rb(1)-O(4)#4	3.025(4)	B(1)-O(3)	1.353(8)
Rb(1)-O(7)#1	3.365(4)	B(1)-O(1)	1.381(8)
Rb(1)-O(7)	3.181(4)	B(1)-O(2)	1.349(7)
Rb(1)-O(2)#4	2.869(4)	B(2)-F(1)	1.468(7)
Rb(1)-O(2)	3.159(4)	B(2)-O(4)	1.442(8)
Rb(2)-F(1)#1	2.935(4)	B(2)-O(3)	1.457(8)
Rb(2)-F(2)#2	2.985(4)	B(2)#1-O(7)	1.467(8)
Rb(2)-F(2)#3	2.916(3)	B(3)-O(5)	1.447(7)
Rb(2)-O(1)#2	2.809(4)	B(3)-O(2)	1.489(7)
Rb(2)-O(6)#3	2.795(4)	B(3)#6-O(8)	1.494(7)
Rb(2)-O(4)#4	3.314(4)	B(3)#9-O(4)	1.472(7)
Rb(2)-O(5)	2.754(4)	B(4)-O(1)	1.459(7)
Rb(2)-O(7)	2.827(4)	B(4)-O(6)	1.454(7)
Rb(3)-F(1)#5	2.852(4)	B(4)-F(2)	1.497(7)
Rb(3)-F(2)#6	2.837(3)	B(4)-O(5)	1.427(7)
Rb(3)-F(2)#7	2.932(4)	B(5)-O(6)	1.369(7)
Rb(3)-O(8)	2.828(4)	B(5)-O(7)	1.365(7)
Rb(3)-O(8)#8	3.031(4)	B(5)-O(8)	1.360(8)
O(3)-B(1)-O(1)	116.0(5)	O(4)-B(2)-O(3)	118.1(5)
O(2)-B(1)-O(3)	124.1(6)	O(4)-B(2)-O(7)#5	113.1(5)
O(2)-B(1)-O(1)	119.9(5)	O(7)#5-B(2)-F(1)	105.4(5)
O(1)-B(4)-F(2)	105.3(5)	O(8)-B(5)-O(6)	117.7(5)
O(6)-B(4)-F(2)	102.6(4)	O(8)-B(5)-O(7)	120.8(5)
O(6)-B(4)-O(1)	110.1(5)	O(7)-B(5)-O(6)	121.5(6)

O(5)-B(4)-F(2)	108.3(5)	O(4)#4-B(3)-O(8)#11	109.8(5)
O(5)-B(4)-O(1)	113.8(5)	O(4)#4-B(3)-O(2)	107.9(4)
O(5)-B(4)-O(6)	115.6(5)	O(5)-B(3)-O(8)#11	109.3(5)
O(3)-B(2)-F(1)	107.2(5)	O(5)-B(3)-O(4)#4	110.7(4)
O(3)-B(2)-O(7)#5	105.2(5)	O(5)-B(3)-O(2)	110.6(5)
O(4)-B(2)-F(1)	106.9(4)	O(2)-B(3)-O(8)#11	108.6(4)

Symmetry transformations used to generate equivalent atoms:

#1 -x+1,y-1/2,-z+1   #2 x,y-1,z   #3 -x+1,y-1/2,-z+2

#4 -x,y-1/2,-z+1   #5 -x+1,y+1/2,-z+1   #6 x+1,y,z

#7 -x+1,y+1/2,-z+2   #8 -x+2,y+1/2,-z+2   #9 -x,y+1/2,-z+1

#10 x,y+1,z   #11 x-1,y,z   #12 -x+2,y-1/2,-z+2

Table S5. Selected bond lengths (Å) and angles (deg.) for $K_{0.6}Rb_{2.4}B_5O_8F_2$.

Rb(1)-O(2)#3	3.365(7)	K(3)-F(1)#2	2.831(5)
Rb(1)-O(2)	3.153(6)	K(3)-F(1)#1	2.981(6)
Rb(1)-O(6)#4	2.869(6)	K(3)-F(2)#3	2.901(6)
Rb(1)-O(6)	3.111(7)	B(1)-O(1)	1.376(12)
Rb(1)-O(7)#1	2.999(6)	B(1)-O(2)	1.336(12)
Rb(1)-O(7)#3	3.093(7)	B(1)-O(3)	1.377(12)
Rb(1)-O(8)#4	3.022(7)	B(2)-O(3)	1.474(12)
Rb(1)-F(2)	2.814(5)	B(2)-O(4)	1.408(12)
Rb(2)-O(1)	2.794(6)	B(2)-O(5)	1.466(12)
Rb(2)-O(1)#7	3.009(7)	B(2)-F(1)	1.496(12)
Rb(2)-O(3)	3.378(7)	B(3)-O(1)#9	1.499(12)
Rb(2)-O(4)#5	2.984(6)	B(3)-O(4)	1.454(11)
Rb(2)-O(8)#6	3.051(6)	B(3)-O(6)	1.476(12)
Rb(2)-F(1)#5	2.896(6)	B(3)-O(8)#4	1.466(12)
Rb(2)-F(1)#8	2.820(5)	B(4)-O(5)	1.382(12)
Rb(2)-F(2)#6	2.812(6)	B(4)-O(6)	1.351(12)
K(3)-O(2)	2.773(7)	B(4)-O(7)	1.342(13)
K(3)-O(3)#2	2.736(7)	B(5)-O(2)#6	1.477(12)
K(3)-O(4)	2.705(7)	B(5)-O(7)	1.465(12)
K(3)-O(5)#1	2.750(6)	B(5)-O(8)	1.437(12)
K(3)-O(8)#4	3.294(6)	B(5)-F(2)	1.458(12)
O(1)-B(1)-O(3)	116.3(9)	O(6)-B(3)-O(1)#9	108.6(8)
O(2)-B(1)-O(1)	120.8(9)	O(8)#4-B(3)-O(1)#9	110.0(7)
O(2)-B(1)-O(3)	122.9(9)	O(8)#4-B(3)-O(6)	108.8(7)
O(3)-B(2)-F(1)	101.5(7)	O(6)-B(4)-O(5)	119.2(9)
O(4)-B(2)-O(3)	115.4(8)	O(7)-B(4)-O(5)	116.3(9)
O(4)-B(2)-O(5)	114.8(8)	O(7)-B(4)-O(6)	124.5(9)

O(4)-B(2)-F(1)	109.6(8)	O(7)-B(5)-O(2)#6	104.9(8)
O(5)-B(2)-O(3)	109.0(8)	O(8)-B(5)-O(2)#6	112.4(8)
O(5)-B(2)-F(1)	105.3(8)	O(8)-B(5)-O(7)	118.8(8)
O(4)-B(3)-O(1)#9	108.9(7)	O(8)-B(5)-F(2)	107.4(8)
O(4)-B(3)-O(6)	110.1(7)	F(2)-B(5)-O(2)#6	104.9(8)
O(4)-B(3)-O(8)#4	110.5(7)	F(2)-B(5)-O(7)	107.5(8)

Symmetry transformations used to generate equivalent atoms:

#1 x,y-1,z   #2 -x+1,y-1/2,-z   #3 -x+1,y-1/2,-z+1

#4 -x+2,y-1/2,-z+1   #5 -x+1,y+1/2,-z   #6 -x+1,y+1/2,-z+1

#7 -x,y+1/2,-z   #8 x-1,y,z   #9 x+1,y,z

#10 -x,y-1/2,-z   #11 x,y+1,z   #12 -x+2,y+1/2,-z+1

Table S6. Assignment of the absorption peaks observed in the IR spectra of $Rb_3B_5O_8F_2$ and $K_{0.6}Rb_{2.4}B_5O_8F_2$:

Mode description	Absorption peaks (cm^{-1}) for $Rb_3B_5O_8F_2$	Absorption peaks (cm^{-1}) for $K_{0.6}Rb_{2.4}B_5O_8F_2$
$v_{as}(BO_3)$	1396, 1327	1389, 1331
$v_{as}(BO_4)$	1177, 1003	1177, 999
$v_{as}(BO_3F)$	1088	1088
$v_s(BO_3)$	937	937
$v_s(BO_4)$	891	895
$v_s(BO_3F)$	779	783
$\delta_{out}(BO_3)$	733, 694	733, 691
$\delta(BO_4, BO_3)$	594, 525	594, 525

Table S7. Investigation of the non-centrosymmetric alkali and alkaline-earth metal fluorooxoborates:

Compounds	Space groups	SHG effect
α-BaBOF$_3$[10]	$P2_1$	no apparent signal
BaB$_2$O$_3$F$_2$[11]	$P2_1$	very weak
Li$_2$B$_3$O$_4$F$_3$[12]	$P2_12_12_1$	no observed
BaB$_4$O$_5$F$_4$[13]	$P2_1$	d_{22}=0
NaB$_4$O$_6$F[14]	$C2$	0.9×KDP
RbB$_4$O$_6$F[15]	$Pna2_1$	0.8×KDP
CsB$_4$O$_6$F[16]	$Pna2_1$	1.9×KDP
NH$_4$B$_4$O$_6$F[17]	$Pna2_1$	3×KDP
CaB$_5$O$_7$F$_3$[18]	$Cmc2_1$	2×KDP
SrB$_5$O$_7$F$_3$[19]	$Cmc2_1$	1.6×KDP
MgB$_5$O$_7$F$_3$[20]	$Cmc2_1$	2.4×KDP
LiB$_6$O$_9$F[21,22]	$Pna2_1$	d_{24}=0.161
Li$_2$B$_6$O$_9$F$_2$[23]	Cc	0.9×KDP
LiNaB$_6$O$_9$F$_2$[24]	$Pnn2$	1.1×KDP
Na$_4$B$_8$O$_9$F$_{10}$[25]	$Pna2_1$	0.7×KDP
CsKB$_8$O$_{12}$F$_2$[15]	$P321$	1.9×KDP
CsRbB$_8$O$_{12}$F$_2$[15]	$P\bar{6}2c$	1.1×KDP
K$_{10}$B$_{13}$O$_{15}$F$_{19}$[26]	$R3m$	0.4×KDP
Rb$_{10}$B$_{13}$O$_{15}$F$_{19}$[26]	$R3m$	0.5×KDP

Fig. S1. The Rb$^+$ cation coordination of Rb$_3$B$_5$O$_8$F$_2$.
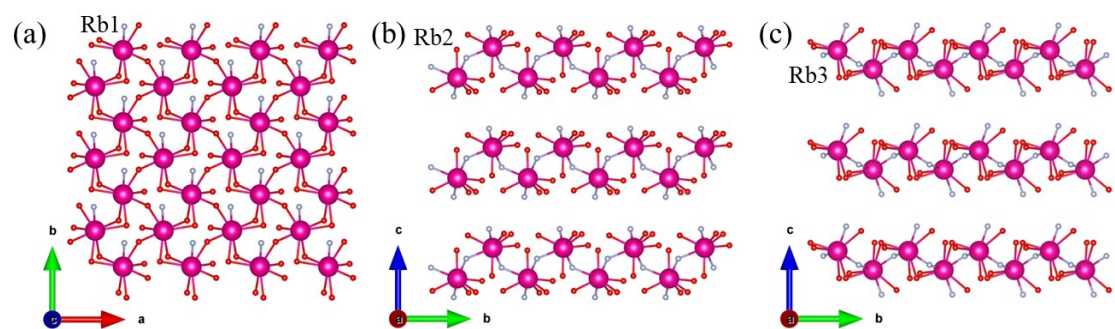
Fig. S2. The frameworks of (a) $Li_2Na_{0.9}K_{0.1}B_5O_8F_2$ and (b) $Rb_3B_5O_8F_2$, respectively (Rubidium pink, lithium bright green, sodium yellow, potassium purple, boron green, oxygen red, fluorine gray).

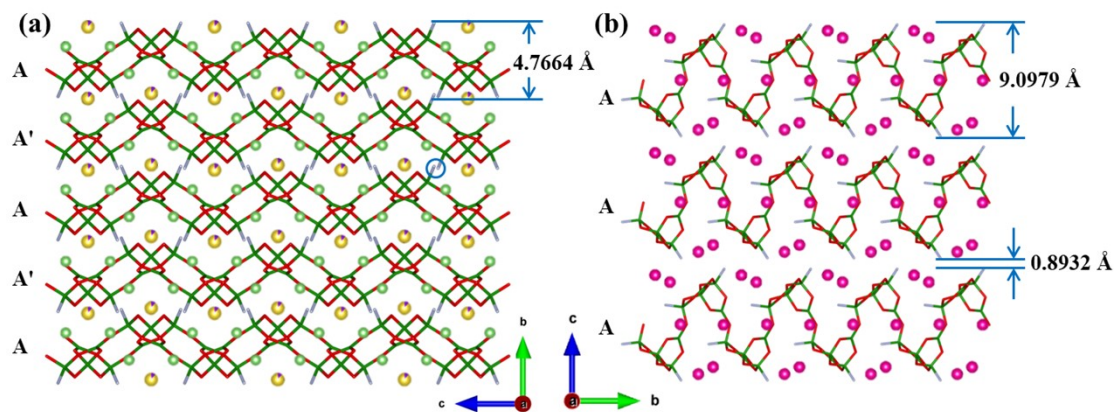Fig. S3. The structure of RbB_5O_8 (a, c) and $Rb_3B_5O_8F_2$ (b,d) (green for boron, red for oxygen, gray for fluorine).
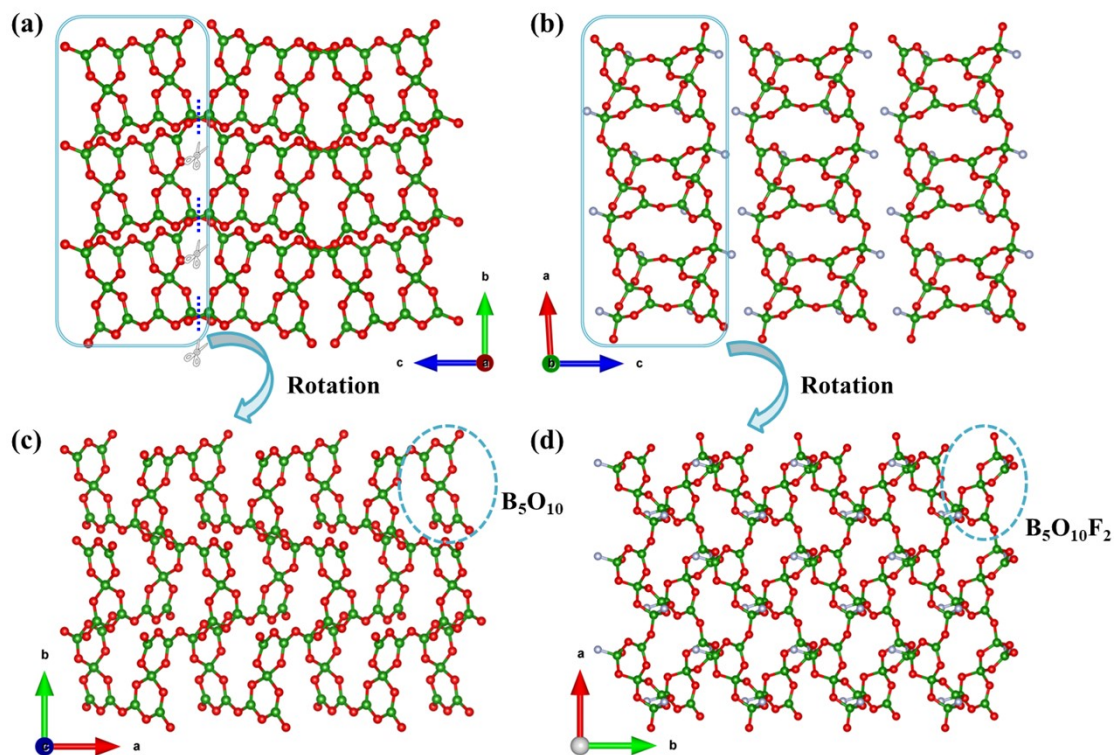
Fig. S4. Powder XRD patterns of (a) $Rb_3B_5O_8F_2$ and (b) $K_{0.6}Rb_{2.4}B_5O_8F_2$.
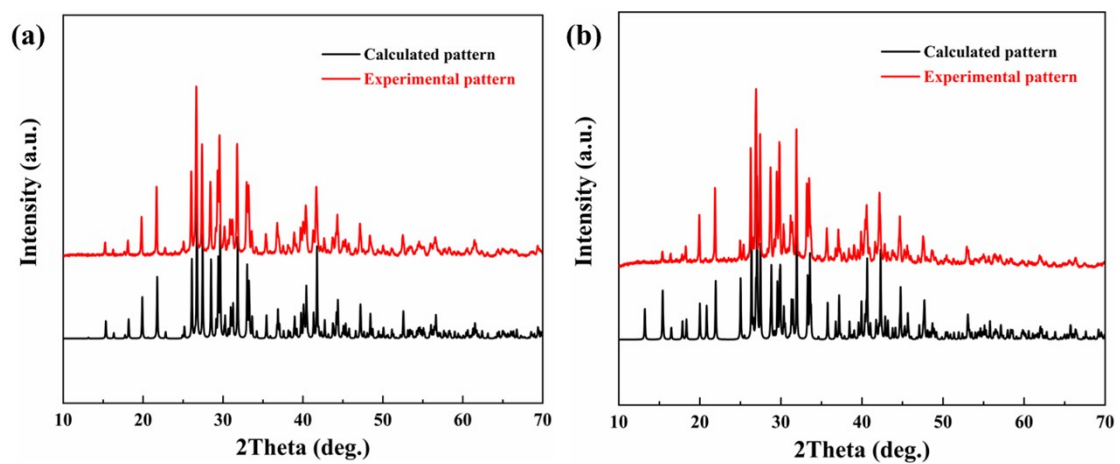
Fig. S5. (a) TG-DSC pattern of $Rb_3B_5O_8F_2$, (b) TG-DSC pattern $K_{0.6}Rb_{2.4}B_5O_8F_2$. (c) Powder XRD patterns of $Rb_3B_5O_8F_2$: calculated one, annealed at 400, 500 °C for 24 h, respectively, (d) Powder XRD patterns of $K_{0.6}Rb_{2.4}B_5O_8F_2$: calculated one, annealed at 400, and 500 °C for 24 h, respectively.
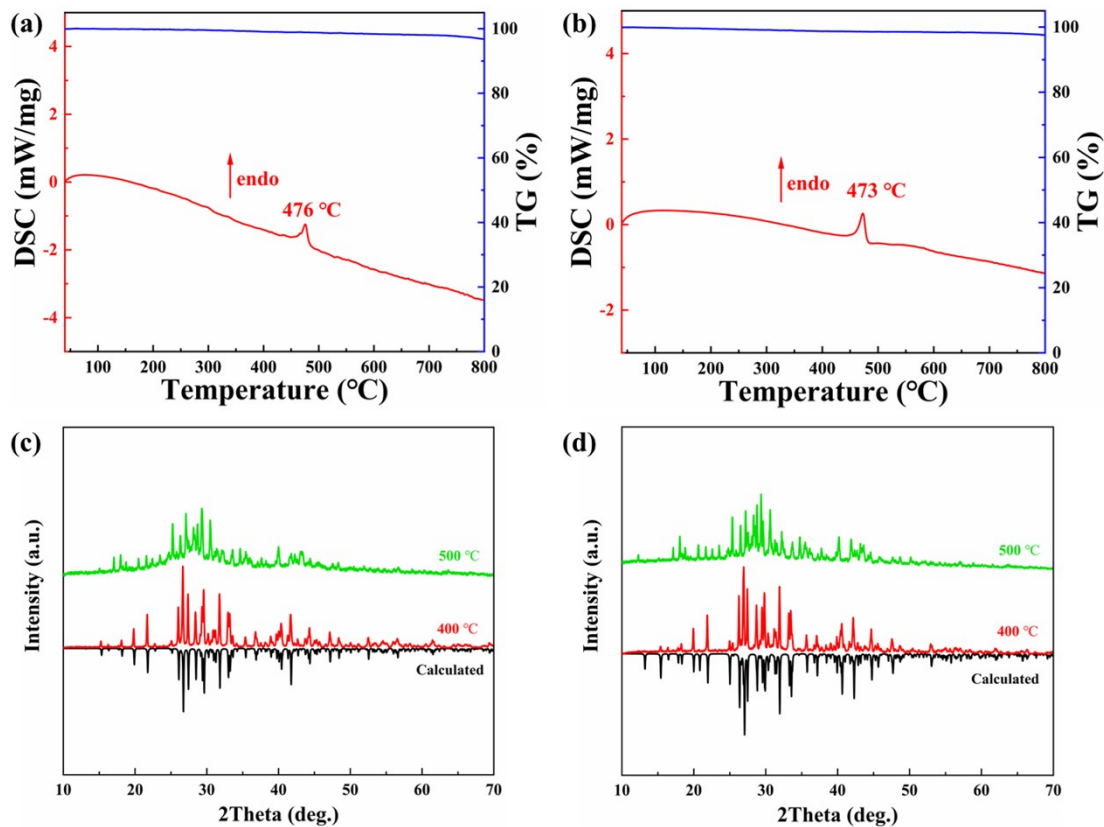
Fig. S6. IR spectra of $Rb_3B_5O_8F_2$ and $K_{0.6}Rb_{2.4}B_5O_8F_2$.
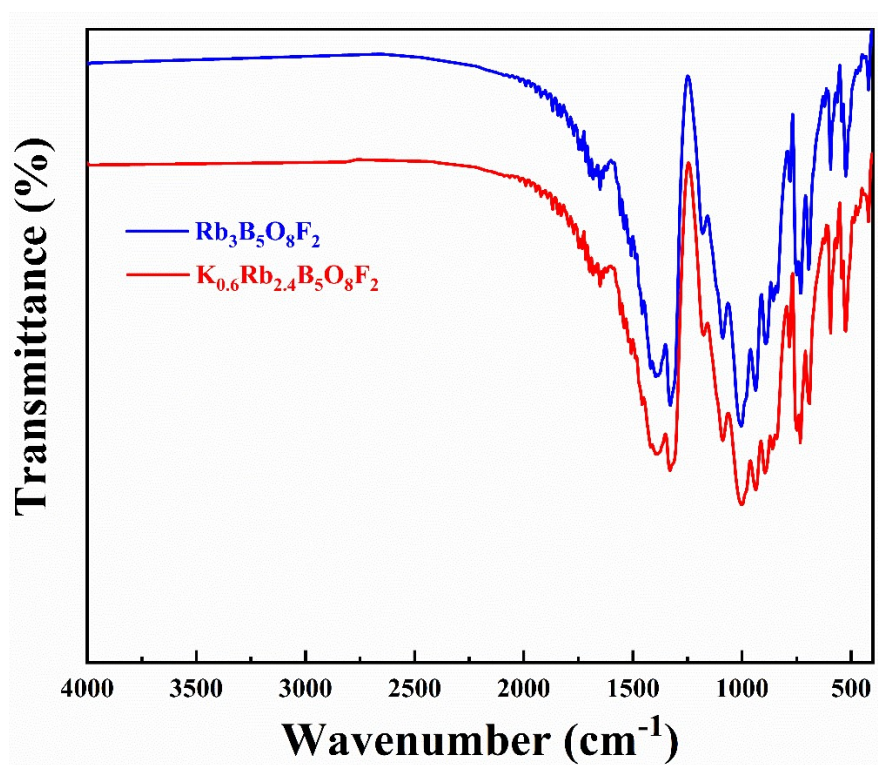
Fig. S7. UV-vis-NIR diffuse reflectance spectra of (a) $Rb_3B_5O_8F_2$ and (b) $K_{0.6}Rb_{2.4}B_5O_8F_2$, respectively.

Fig. S8. EDX spectroscope of $K_{0.6}Rb_{2.4}B_5O_8F_2$. The EDX spectroscope demonstrates the existence of K, Rb, B, O and F elements in $K_{0.6}Rb_{2.4}B_5O_8F_2$.
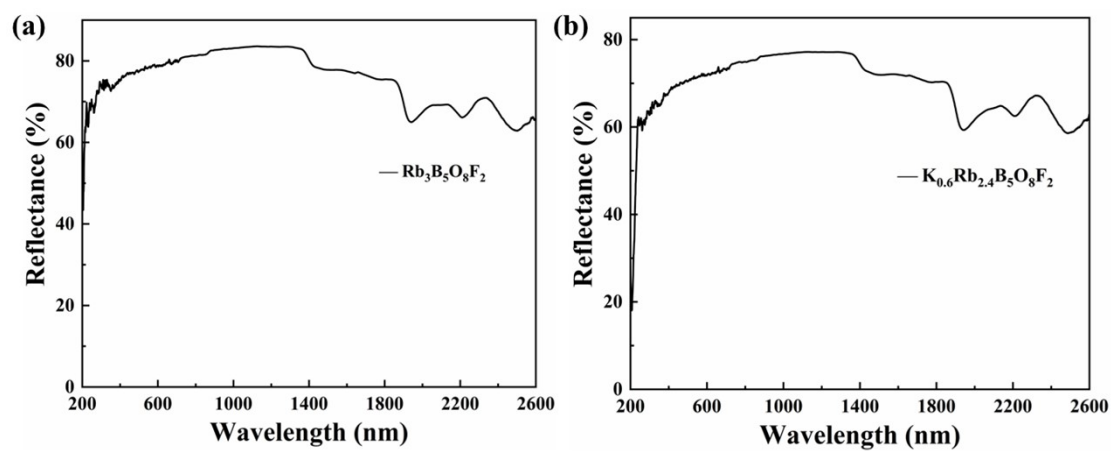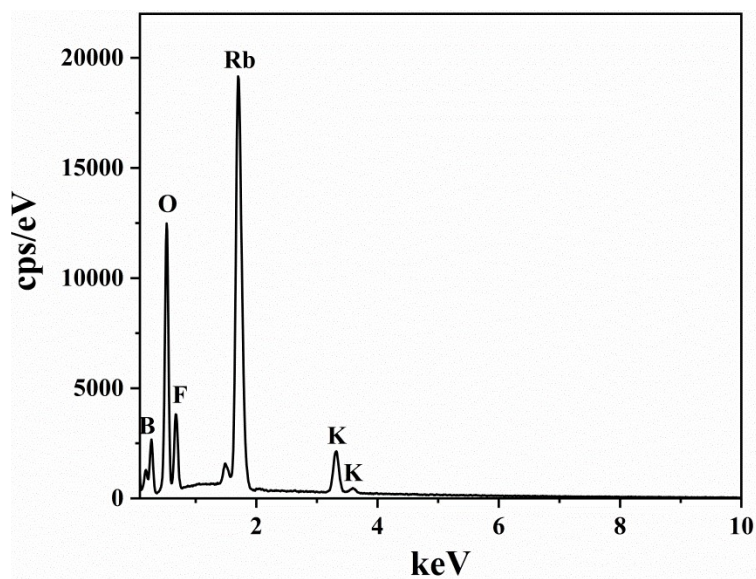
References

1   SAINT, *version 7.60A*, Bruker Analytical X-ray Instruments, Inc., Madison, WI, 2008.

2   O. V. Dolomanov, L. J. Bourhis, R. J. Gildea, J. A. K. Howard and H. Puschmann, OLEX2: A complete structure solution, refinement and analysis program, *J. Appl. Crystallogr.* 2009, **42**, 339−341.

3   A. L. Spek, Single-crystal structure validation with the program PLATON, *J. Appl. Crystallogr.*, 2003, **36**, 7−13.

4   S. K. Kurtz and T. T. Perry, A powder technique for the evaluation of nonlinear optical materials, *J. Appl. Phys.*, 1968, **39**, 3798−3813.

5   S. J. Clark, M. D. Segall, C. J. Pickard, P. J. Hasnip, M. J. Probert, K. Refson and M. C. Payne, First principles methods using CASTEP, *Z. Kristallogr.*, 2005, **220**, 567−570.

6   B. G. Pfrommer, M. Côté, S. G. Louie and M. L. Cohen, Relaxation of crystals with the quasi-Newton method, *J. Comput. Phys.*, 1997, **131**, 233-240.

7   J. P. Perdew, K. Burke and M. Ernzerhof, Generalized dradient approximation made simple, *Phys. Rev. Lett.*, 1996, **77**, 3865.

8   J. S. Lin, A. Qteish, M. C. Payne and V. Heine, Optimized and transferable nonlocal separable *ab initio* pseudopotentials, *Phys. Rev. B*, 1993, **47**, 4174.

9   A. M. Rappe, K. M. Rabe, E. Kaxiras and J. D. Joannopoulos, Optimized pseudopotentials, *Phys. Rev. B*, 1990, **41**, 1227.

10   K.T. Liu, J. Han, T. Baiheti, F. M. Li, Z. L. Wei, Z. H. Yang, M. Mutailipu and S. L. Pan, Finding a series of $BaBOF_3$ fluorooxoborate polymorphs with tunable symmetries: A simple but flexible case, *Chem. Mater.*, 2021, **33**, 7905−7913.

11   C. M. Huang, F. F. Zhang, H. Li, Z. H. Yang, H. H. Yu and S. L. Pan, $BaB_2O_3F_2$: A barium fluorooxoborate with a unique $_{\infty}^{2}[B_2O_3F]^-$ layer and short cutoff edge, *Chem. – Eur. J.*, 2019, **25**, 6693−6697.

12   T. Pilz, H. Nuss and M. Jansen, $Li_2B_3O_4F_3$, a new lithium-rich fluorooxoborate, *J. Solid State Chem.*, 2012, **186**, 104−108.

13 W. B. Zhang, S. R. Guo, S. J. Han, L. Y. Wang, X. Zhou, Z. H. Yang and S. L. Pan, $BaB_4O_5F_4$ with reversible phase transition featuring unprecedented fundamental building blocks of $[B_{16}O_{21}F_{16}]$ in the α-phase and $[B_4O_6F_4]$ in the β-phase, *Chem. Commun.*, 2021, **57**, 4182−4185.

14 Z. Z. Zhang, Y. Wang, B. B. Zhang, Z. H. Yang and S. L. Pan, Polar fluorooxoborate, NaB_4O_6F: A promising material for ionic conduction and nonlinear optics, *Angew. Chem. Int. Ed.*, 2018, **57**, 6577−6581.

15 Y. Wang, B. B. Zhang, Z. H. Yang and S. L. Pan, Cation-tuned synthesis of fluorooxoborates: Towards optimal deep-ultraviolet nonlinear optical materials, *Angew. Chem. Int. Ed.*, 2018, **57**, 2150−2154.

16 X. F. Wang, Y. Wang, B. B. Zhang, F. F. Zhang, Z. H. Yang and S. L. Pan, CsB_4O_6F: A congruent-melting deep-ultraviolet nonlinear optical material by combining superior functional units, *Angew. Chem. Int. Ed.*, 2017, **56**, 14119−14123.

17 G. Q. Shi, Y. Wang, F. F. Zhang, B. B. Zhang, Z. H. Yang, X. L. Hou, S. L. Pan and K. R. Poeppelmeier, Finding the next deep-ultraviolet nonlinear optical material: $NH_4B_4O_6F$, *J. Am. Chem. Soc.*, 2017, **139**, 10645−10648.

18 Z. Z. Zhang, Y. Wang, B. B. Zhang, Z. H. Yang and S. L. Pan, $CaB_5O_7F_3$: A beryllium-free alkaline-earth fluorooxoborate exhibiting excellent nonlinear optical performances, *Inorg. Chem.*, 2018, **57**, 4820−4823.

19 M. Mutailipu, M. Zhang, B. B. Zhang, L. Y. Wang, Z. H. Yang, X. Zhou and S. L. Pan, $SrB_5O_7F_3$ functionalized with $[B_5O_9F_3]^{6-}$ chromophores: Accelerating the rational design of deep-ultraviolet nonlinear optical materials, *Angew. Chem. Int. Ed.*, 2018, **57**, 6095−6099.

20 M. Xia, F. M. Li, M. Mutailipu, S. J. Han, Z. H. Yang and S. L. Pan, Discovery of first magnesium fluorooxoborate with stable fluorine terminated framework for deep-UV nonlinear optical application, *Angew. Chem. Int. Ed.*, 2021, **60**, 14650−14656.

21 G. Cakmak, J. Nuss and M. Jansen, LiB_6O_9F, the first lithium fluorooxoborate-crystal structure and ionic conductivity, *Z. Anorg. Allg. Chem.*, 2009, **635**,

631−636.

22　B. Andriyevsky, K. Doll, G. Cakmak, M. Jansen, A. Niemer and K. Betzler, DFT-based *ab initio* study of structural and electronic properties of lithium fluorooxoborate LiB_6O_9F and experimentally observed second harmonic generation, *Phys. Rev. B*, 2011, **84**, 125112.

23　B. B. Zhang, G. Q. Shi, Z. H. Yang, F. F. Zhang and S. L. Pan, Fluorooxoborates: beryllium-free deep-ultraviolet nonlinear optical materials without layered growth, *Angew. Chem. Int. Ed.*, 2017, **56**, 3916−3919.

24　X. J. Li, Z. L. Chen, F. M. Li, F. F. Zhang, Z. H. Yang and S. L. Pan, $LiNaB_6O_9F_2$: A promising UV NLO crystal having fluorine-directed optimal performances and double interpenetrating $^3[B_6O_9F_2]_\infty$ networks, *Adv. Opt. Mater.*, 2022, DOI: 10.1002/adom.202202195.

25　H. H. Cheng, F. M. Li, Z. H. Yang and S. L. Pan, $Na_4B_8O_9F_{10}$: A deep-ultraviolet transparent nonlinear optical fluorooxoborate with unexpected short phase-matching wavelength induced by optimized chromatic dispersion, *Angew. Chem. Int. Ed.*, 2022, **61**, e202115669.

26　W. Y. Zhang, Z. L. Wei, Z. H. Yang, and S. L. Pan, Noncentrosymmetric fluorooxoborates $A_{10}B_{13}O_{15}F_{19}$ (A = K and Rb) with unexpected $[B_{10}O_{12}F_{13}]^{7-}$ units and deep-ultraviolet cutoff edges, *Inorg. Chem.*, 2020, **59**, 3274−3280.